PCCP

Accepted Manuscript

ROYAL SOCIETY OF CHEMISTRY

www.rsc.org/pccp

Functionalization of nanostructured cerium oxide films with histidine

Nataliya Tsud[1*], Sofiia Bercha[1], Robert G. Acres[2], Mykhailo Vorokhta[1], Ivan Khalakhan[1], Kevin C. Prince[2,3,4], Vladimír Matolín[1]

[1] Charles University, Faculty of Mathematics and Physics, Department of Surface and Plasma Science, V Holešovičkách 2, Prague, 18000, Czech Republic

[2] Elettra-Sincrotrone Trieste S.C.p.A., in Area Science Park, Strada Statale 14, km 163.5, Basovizza (Trieste), 34149, Italy

[3] CNR-IOM Laboratorio TASC, Basovizza (Trieste), 34149, Italy

[4] eChemistry Laboratory, Department of Chemistry and Biotechnology, School of Science, Faculty of Science, Engineering and Technology, Swinburne University of Technology, Melbourne, Victoria 3122, Australia.

[*] corresponding author Nataliya.Tsud@mff.cuni.cz

Abstract

The surfaces of polycrystalline cerium oxide films were modified by histidine adsorption in vacuum and characterized by the synchrotron based techniques of core and valence level photoemission, resonant photoemission and Near Edge X-ray Absorption Spectroscopy, as well as Atomic Force Microscopy. The histidine is strongly bound to the oxide surface in anionic form through the deprotonated carboxylate group, and forms a disordered molecular adlayer. The imidazole ring and the amino side group do not form bonds with the substrate but are involved in the intermolecular hydrogen bonding which stabilizes the molecular adlayer. The surface reaction with histidine results in water desorption accompanied by oxide reduction, which is propagated into the bulk of the film. Previously studied, well characterized surfaces are a guide to the chemistry of the present polycrystalline surface and histidine bonds via the carboxylate group in both cases. In contrast, bonding via the imidazole group occurs on the well-ordered surface but not in the present

case. The morphology and structure of the cerium oxide are decisive factors which define the adsorption geometry of the histidine adlayer.

Introduction

Knowledge of the binding mechanism of biomolecules to inorganic materials is a key factor in the efficient design of third generation mediator-less enzymatic biosensors. The major demand for sensors with improved sensitivity and detection limits originates from the healthcare industry, [1-5] and research in this field is multidisciplinary, spanning biochemistry, physical chemistry, electronics and engineering. The understanding of a bio-interface on the elementary level is usually limited because of the complexity of real enzymes and their reaction with the analyte molecules.

In recent years, an increasing amount of work has been devoted to the development and construction of bio-electrodes based on nanostructured cerium oxide films for control and detection of glucose, [6] triglyceride, [7] cholesterol, [8] hydrogen peroxide [9,10] and glutamic acid. [11] The active part of these biosensors is formed by corresponding enzyme molecules dispersed on nanostructured CeO_2 film. Several techniques such as electrochemistry, X-ray diffraction, infrared spectroscopy, scanning electron and atomic force microscopies have been employed for examination of enzyme immobilization on CeO_2. [6-10] An important challenge in the development of electrochemical biosensors is to establish satisfactory electrical communication between the active sites of the enzyme and the oxide electrode surface. Advances in achieving direct electron transfer, the main feature of the third generation of biosensors, can be made by modification of the electrode surface with a nanostructured oxide. [1, 2]

In view of the importance of nanostructured cerium oxide in various biological applications, the potential of this material in medicine has been widely explored. Cerium oxide nanoparticles are known as effective radioprotective agents for normal tissues. [12] They also show a differential protection in normal cells as compared to tumor cells. [13] Organism aging and disease often overtax the system and free radical generation exceeds the organism's natural antioxidant capacity, resulting

in a state termed oxidative stress. Cerium oxide nanoparticles appear to hold promise for nano pharmacotherapy of neurodegenerative and other disorders linked to this oxidative stress. [14-16]

In the present work we studied the adsorption of the amino acid histidine. Histidine plays an important role in many metalloproteins providing a binding site for coordinated metal complexes, for example Fe porphyrins. [17-19] The imidazole ring of histidine is an essential ligand for hemoglobin and myoglobin functionality, and in general it shows excellent binding abilities toward metal ions. [17, 20] The latter feature is widely explored for the development of electrochemical sensors based on peptide modified electrodes for metal detection in environmental monitoring. [21-23] Promising sensing characteristics were obtained for histidine containing molecules e.g. short peptides Gly–Gly–His [22] or biohomopolymer poly-histidine [23] grafted to the electrode surface via self-assembled monolayer of silanes, alkanethiols or aryl diazonium salts. It was shown, for instance, that the tripeptide Gly–Gly–His readily binds to Cu^{2+} ions at ultralow concentrations through the imidazole group. [22] Heme functionalized electrode surfaces are another example of potential biosensors for diatomic molecules such as CO, NO, O_2. Fe porphyrins on Ag(111) [24] or silane modified SiO_2 [25] demonstrate high sensitivity to NO. Due to the complexity of the chemical structure, the contribution of the imidazole ligand to the sensing abilities of the Fe porphyrins was mainly studied theoretically, for example Ref. [26]

Recently we studied histidine interaction with model, well-ordered cerium oxide films (0.15 nm thick) on Cu(111), wherein both molecular adsorption and oxide preparation were done in vacuum. [27] Histidine, one of the principal amino acids, was chosen with the aim to model the bonding of proteins and other complex biomolecules with the cerium oxide surface. The structure of the histidine molecule is shown in Figure 1, and it has three important chemical groups: carboxylic acid, α-amino and imidazole. It was shown that histidine binds to CeO_2 in anionic form as His^{2-}. Three functional groups contribute to the strong bond formation: the carboxylate group, imidazole ring (IM) and the α-amino group. The imino nitrogen atom of the IM ring, carboxylic oxygen atoms and the α-amino nitrogen interact with the cerium oxide surface right after deposition. The

deprotonation of the IM amino nitrogen was shown to depend on the concentration of the Ce^{4+} cations on the surface and was thermally induced. For 1 ML His/CeO_2 the imidazole ring was shown to be almost parallel to the surface. Mutual charge exchange between the histidine molecule and the oxide was observed, and was connected with the increased concentration of the Ce^{3+} centers on the CeO_2 surface. [27]

Here we present the continuation of this line of research. The next step toward practical application of cerium oxide for biosensing devices comprises the use of technologically more accessible nanostructured material. In this work cerium oxide prepared by nonreactive magnetron sputtering was chosen as a model substrate. This material is characterized by high oxygen atom mobility [28] and in combination with platinum additives is promising for fuel cell applications because of its high specific power, low cost and planar deposition techniques. [29] The goal of this work is to increase the basic understanding of phenomena and properties of planar nano-scale size CeO_2 systems with respect to bonding with histidine.

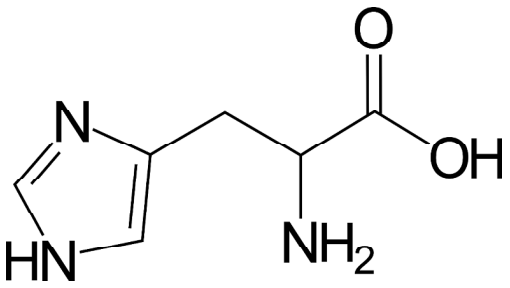

Fig. 1. Schematic structure of histidine ($C_6H_9N_3O_2$).

Experimental

The ceria films (20 nm thick) were prepared ex-situ by the nonreactive magnetron sputtering of a CeO_2 target (99.99 %, Kurt J. Lesker). The sputtering was carried out in an Ar atmosphere at total pressure of $4x10^{-3}$ mbar with RF power of 80 W giving a growth rate of the cerium oxide film of 1 nm/min. The films were deposited onto a single-crystalline Si(100) wafer covered by a 4 nm thick

natural oxide film. The morphology of the CeO_2 films was examined by means of a Bruker MultiMode 8 Atomic Force Microscope (AFM).

The experiment was performed at the Materials Science Beamline at the Elettra-Sincrotrone Trieste light source; for further details see Ref. [27] The C 1s, N 1s and O 1s core levels were acquired with photon energy 410, 475 and 630 eV and total resolution 350, 500 and 700 meV, respectively. The valence band spectra were recorded at 115, 121.4 and 124.8 eV (to monitor Ce 4d→4f resonances in Ce cations), with total resolution 190 meV measured as the width of the Fermi edge of Cu(111). Spectra measured at 121.4 and 124.8 eV correspond to the D(Ce^{3+}) resonant enhancements in Ce^{3+} cations (emission from Ce 4f states located at binding energy (BE) about 1.4 eV) and D(Ce^{4+}) - in Ce^{4+} cations (emission from hybridized oxygen cerium states at about 4.0 eV), respectively. [30] The valence band spectrum measured at photon energy of 115 eV corresponds to off resonance for both Ce^{3+} and Ce^{4+} states and was used as a reference for intensity subtraction between the corresponding features on- and off-resonance. The D(Ce^{3+})/D(Ce^{4+}) resonant enhancement ratio (RER) gives direct information about the oxidation state of surface cerium ions. [30] Al Kα radiation (1486.6 eV) was used to measure the core levels of C 1s, N 1s, O 1s, Ce 3d, Si 2p region for CeO_2 films and C 1s, N 1s, O 1s, Cu $2p_{3/2}$ for a Cu(111) reference sample, with total resolution of 1 eV. No Si 2p signal was detected on CeO_2. Charging was observed on CeO_2 and led to a peak shift of about 1 eV to high BE. The binding energies of the XPS spectra were corrected using the position of the Ce 3d peak component at 916.7 eV as a reference. [27, 31] The corrected positions of core levels were then used as the reference for lines measured with the synchrotron radiation. The emission angle for the photoelectrons was 0º and 20º with respect to the sample normal for synchrotron light and the X-ray source, respectively. The intensity of the photoelectron spectra measured with synchrotron radiation was normalized to the incident photon flux. The precision of the photon energy settings was verified by measuring the Fermi edge on a clean Cu(111) surface. The core level spectra were fitted with Voigt or Gaussian profiles after proper background subtraction. All photoemission data were processed using the KolXPD fitting software. [32]

After insertion into vacuum the CeO_2 films were cleaned by light Ar ion sputtering (500 V, 10 min) and annealing in O_2 (5x 10^{-7} mbar total pressure) at 250° C for 15 min to restore the surface stoichiometry. Such a treatment gives a clean surface with negligible contribution of Ce^{3+} centers (the RER ratio for the clean surface was 0.05 compared to 0 for perfect CeO_2). No carbon signal was detected.

The Cu(111) crystal, used as a reference substrate, (MaTecK GmbH, 8 mm diameter, 2 mm thickness, 99.999%) was cleaned by several cycles of Ar ion sputtering and annealing to 450° C. No impurities, such as carbon or oxygen, were detected by photoemission on the Cu(111) surface, and a sharp (1×1) LEED pattern was observed before histidine adsorption.

L-Histidine $C_6H_9N_3O_2$ (≥99.5%) was supplied by Sigma-Aldrich and used without further purification. Histidine was deposited by evaporation from a Knudsen cell in vacuum. Before deposition, the histidine powder in the crucible was degassed in vacuum at 110° C and then dosed at 125° C onto the substrate at 25° C. The deposition rate was checked on Cu(111) and found to be about 1 monolayer (ML) per 100 seconds, determined from analysis of the photoemission data. [27] The local pressure during deposition was about 3×10^{-8} mbar. The ceria or Cu(111) substrates, after preparation in the experimental chamber, were transferred to the preparation chamber for molecular deposition.

NEXAFS spectra were taken at the N K-edge using the nitrogen KVV Auger yield, at normal (NI, 90º) and 30º (coincides with the normal emission (NE) for photoelectrons) incidence of the photon beam with respect to the surface. The raw NEXAFS spectra were normalized to the intensity of the photon beam, measured by means of a high transmission gold mesh simultaneously with the sample measurement. Then the corresponding background spectra of the clean sample recorded under identical conditions were subtracted. The energy resolution for the N K-edge NEXAFS spectra was estimated to be 0.38 eV. The polarization of light from the beamline has not been measured, but is believed to be between 80 and 90 % linear, as the source is a bending magnet.

We checked for radiation damage by monitoring the C 1s peak. No spectral changes were observed during one experimental step, i.e. stable C 1s signal for about 25 min. For the next experimental step a new point on the sample surface was analyzed. The homogeneity of the O 1s signal was checked before adsorption of histidine.

Results and discussion

The CeO_2 film prepared by magnetron sputtering has polycrystalline structure with a grain size between 10 and 30 nm. Figure 2 shows the AFM 3D image of an as prepared CeO_2 film. The surface roughness was about 1.50 nm. As stated, before deposition of histidine in UHV the surface was cleaned by light Ar ion sputtering followed by re-oxidation in O_2. This treatment decreases the surface roughness by about 20 %, i.e., from 1.50 nm it changed to 1.22 nm.

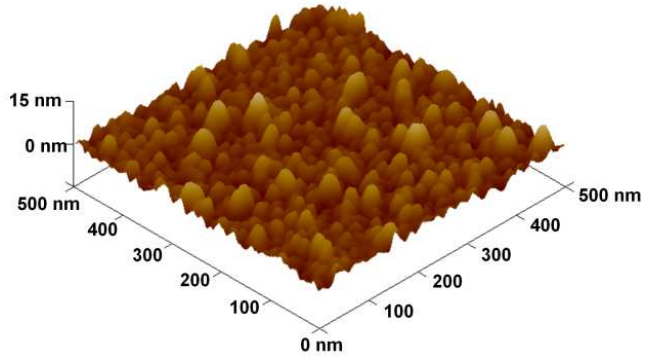

Fig. 2. Three dimensional rendition of an AFM image of the CeO_2 film.

The level of oxidation and stoichiometry of the film were examined by measuring Ce 3d core level and valence band spectra. The high kinetic energy Ce 3d photoelectrons provide average information about oxidation state of Ce cations within the whole oxide film, whereas the resonance enhancement of the Ce 4f valence level is extremely surface sensitive and allows monitoring of surface changes. The Ce 3d spectra of the clean CeO_2 film (Fig. 3a-i) were fitted with three doublets using the Voigt profile after background subtraction. [30] No Ce^{3+} component was observed in the Ce

3d signal before histidine adsorption. The only detected traces of the Ce^{3+} cations were observed in the resonantly enhanced VB spectra, giving a RER ratio of 0.05.

Saturation coverage of histidine on CeO_2 film was obtained after 180 s of deposition. The molecular adlayer thickness on polycrystalline CeO_2 was estimated by comparison of absolute C 1s and N 1s intensities of the histidine saturated coverage on the Cu(111) reference surface. The histidine adlayer on Cu(111) was prepared as in Ref. [27], i.e. more than one monolayer was deposited and then flashed to 100° C to desorb weakly bound species. The spectra were similar to those published. [27] From the attenuation of the copper substrate signal the histidine effective film thickness was found to be ~4.4 Å. This is in good agreement with values estimated for saturated coverage of histidine on Cu(111) and partially reduced ceria on Cu(111), published previously. [27] For the histidine adlayer on the polycrystalline CeO_2 film, the area of the C 1s and N 1s peaks was 6% higher than on the reference Cu(111) sample, so in this case the effective thickness of the saturated coverage was comparable with that on Cu(111). No sign of multilayer film formation was observed (e.g., the presence of the zwitterionic histidine species component in the N 1s core level at BE about 402 eV [27]). After histidine adsorption the substrate was stepwise annealed for one minute at temperatures of 100°, 150° and 200° C. The RER ratio calculated using resonance enhancement of Ce^{3+} and Ce^{4+} features in the valence band, and the Ce^{3+}/Ce^{4+} component ratio calculated by fitting of the Ce 3d spectra (Fig. 3a) versus annealing temperature are shown in Figure 3b. This figure also shows the dependence of RER for the clean oxide film which was treated in the same way as the histidine covered CeO_2. It is worth noting that the clean substrate itself does not change oxidation state with the same thermal treatment as for His/CeO_2. The histidine adsorption affects first the RER ratio (see Fig. 3b), which rises from 0.05 to 0.62, while the Ce^{3+}/Ce^{4+} (Ce 3d) ratio remains 0. So the concentration of the Ce^{3+} centers on the surface increases leaving the deeper oxide layers unaffected. Thermal treatment of the histidine adlayer on CeO_2 results in further oxide reduction which propagates into the bulk of the film (both ratios increase). It is well illustrated by the shape of the Ce 3d core level (Fig. 3a-ii) where the visible contribution of Ce^{3+} states was distinguished after

flashing to 100° C, with the Ce^{3+}/Ce^{4+} (Ce 3d) ratio of 0.08. By annealing to 150° C, the oxide reduction continues apparently from the surface to the bulk (Fig. 3b). Reduction can have two possible origins: desorption of oxygen in the form of water molecules, or electronic character, i.e. charge transfer from histidine molecules to Ce^{4+} centers. The total intensity of the O 1s core level measured with 1486.6 eV photons is strongly reduced after histidine adsorption and 100° C treatment (see Fig. 3c), which favors the model of oxygen loss from the surface. The oxygen intensity behavior will be further discussed in detail below.

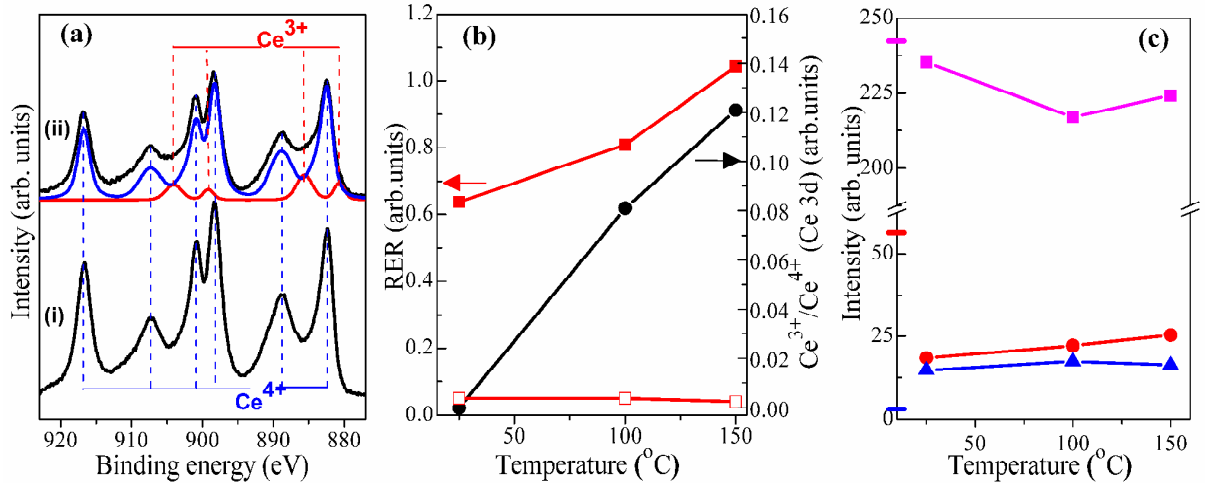

Fig. 3. (a) Ce 3d core levels of (i) clean CeO_2 film and (ii) histidine adlayer on CeO_2 after annealing for one minute at 100° C, where blue and red lines correspond to Ce^{4+} and Ce^{3+} species, respectively. (b) $D(Ce^{3+})/D(Ce^{4+})$(VB) (red filled squares) and Ce^{3+}/Ce^{4+}(Ce 3d) (black filled circles) intensity ratio dependence versus annealing temperature of a histidine covered CeO_2 film. The red open squares correspond to the $D(Ce^{3+})/D(Ce^{4+})$(VB) ratio for the clean CeO_2 film. (c) O 1s core level intensity after deposition of histidine at 25° C and after annealing at 100° C and 150° C: violet line – total O 1s intensity, photon energy 1486.6 eV; red and blue lines – the intensities of O 1s components, photon energy 630 eV, red circles correspond to the peak at 529.5 eV (lattice oxygen) and blue triangles to the peak around 532 eV. The marks of the corresponding color on the vertical axis are the oxygen intensities of the clean substrate before histidine deposition.

NEXAFS spectra of histidine saturated coverage on polycrystalline ceria film are shown in Figure 4 for two different geometries, normal incidence and normal emission. Two characteristic regions of π^* and σ^* resonances are easily distinguishable. The sharp peaks A and B account for the N 1s core excitation to π^* unoccupied molecular orbitals and are assigned to imino and amino nitrogen atoms of the imidazole ring, respectively. [27] The broad features C and D are linked to the 1s $\rightarrow$ σ^* resonances of all nitrogen atoms of histidine. No big difference was detected between the two geometries for any temperature, which indicates a disordered molecular overlayer on the polycrystalline cerium oxide surface. The photon energy of peaks A and B are collected in Table 1. The presence of two peaks after histidine adsorption confirms the fact that the nitrogen atoms of the imidazole ring are in different chemical states. The energies of peaks A and B are systematically lower than values observed for histidine adlayers on an ordered CeO_2(111)/Cu(111) film (see Table 1). We associate the lower energy of the π^* resonances with the presence of the OH groups on the surface of the oxide film. From the available data, we cannot determine whether the interaction is direct, such as hydrogen bonding for instance, or indirect, for example via the substrate. Nyberg et al.[33] reported "surprisingly large effects" in the NEXAFS spectra of glycine/Cu(110) due to hydrogen bonding, and so it is credible that effects may be present in the present case.

The energy separation between A and B is 1.7 eV for histidine adsorbed on polycrystalline ceria. For histidine on epitaxial CeO_2 at 25° C, the values were 1.2 and 1.8 eV for strongly and weakly bonded imino nitrogen atoms. We conclude that on polycrystalline ceria imino nitrogen is not bonded to the surface. The amino nitrogen of the IM ring remains protonated at 25° C and there is negligible change even after 100° C treatment (see Fig. 4). Treatment at 150° C and higher temperature causes a decrease of the π^* resonance B. This finding is explained by thermally induced deprotonation of the amino nitrogen of the IM ring as a result of strong binding to the oxide surface and in line with our previous study of histidine on CeO_2(111)/Cu(111). [27] The deprotonation starts

at 150° C and occurs to a much smaller extent on the polycrystalline film than for the epitaxial ceria surface. [27]

Table 1. NEXAFS spectral features in the π^* resonance range of N K-edge: photon energy of peaks, the energy difference between them Δ. For details see text.

	A, eV	B, eV	Δ (B-A), eV
Assignment	IM imino N	IM amino N	---
His/CeO_2, 25 °C	399.5	401.2	1.7
His/CeO_2, 100 °C	399.5	401.2	1.7
His/CeO_2, 150 °C	399.5	401.3	1.8
His/CeO_2, 200 °C	399.6	401.5	1.9
His/CeO_2/Cu(111), 25 °C [27]	400.8 (400.2)	402.0	1.2 (1.8)
His/CeO_2/Cu(111), 100 °C [27]	400.9	402.0	1.1
His/$CeO_{1.9}$/Cu(111), 100 °C [27]	400.4 (400.2)	401.9	1.5 (1.7)

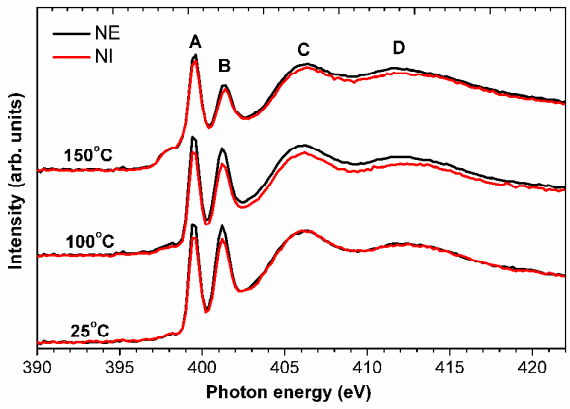

Fig. 4. N K-edge NEXAFS spectra of histidine adsorbed on CeO_2 film. Black and red lines label the spectra measured at normal emission and normal incidence, respectively.

The photoelectron spectra of nitrogen and carbon (Fig. 5) are very similar to those observed for histidine adlayers on CeO_2(111)/Cu(111). [27] The N 1s core level has two visible components after histidine adsorption, which change only slightly with thermal treatment. The component at low binding energy is about 2 and 2.2 times higher than the one at high binding energy for histidine adlayers at 25° C and after annealing to 100° C, respectively. Taking into account the presence of the two different nitrogen atoms of the IM ring in the NEXAFS data we assign the peak at 400.8 eV to amino nitrogen of the IM ring and the component at about 399.5 eV to imino nitrogen of the IM ring and amino side group nitrogen atom which are engaged in hydrogen bonding. A similar effect for an amino group bonding via hydrogen atoms was observed on glycyl-glycine adsorption on Cu(110) and was confirmed by theoretical calculations.[34] The hydrogen bonding may be to the surface or to other molecules. As in the previous study, [27] from the photoemission we cannot distinguish between non-bonded or weakly bonded imino nitrogen of the IM ring. The energy difference between two main π^* resonances and absence of angular dependence indicate that the IM ring is most likely not bound to the oxide surface. The hydrogen atoms of the neighboring histidine molecules probably participate in stabilizing the IM ring far from the surface by means of a network of intermolecular hydrogen bonds. Intramolecular hydrogen bonds in the gas phase can cause shifts of up to 0.7 eV, [35, 36] and it is reasonable to expect stronger hydrogen bonding and shifts on the surface, where the molecules are less constrained. The present conclusion is also supported by C 1s data, see below.

The treatment at 100° C causes a shift of both N 1s components to higher binding energy by about 0.15 eV. Thermal annealing at 150° C causes the appearance of a component at 398.4 eV which was assigned to the deprotonated amino nitrogen atoms of the IM ring bound to the ceria surface. A small reduction of intensity is also observed for the amino nitrogen component, in line with the NEXAFS data. Further temperature increase resulted in decomposition and partial desorption of the molecule (data not shown).

The C 1s core level (Fig. 5b) has two characteristic components for the histidine adlayer on the polycrystalline ceria film, which correspond to carboxylate COO^- and 5 other carbon atoms. The binding energy of 288.7 eV for the COO^- component proves that this group is deprotonated, which is the expected behavior for histidine bound on oxides, accompanied by OH group formation [27 and references therein]. This value is in good agreement with the published values for the COO^- group of alanine on ZnO(1010) (288.8 eV) [37] and proline on TiO_2(110) (288.4 eV). [38] The centroid of the peak corresponding to other carbons is at about 286 eV, in good agreement with the results of histidine on CeO_2(111)/Cu(111). [27] Because of the polycrystalline substrate and disordered molecular overlayer, we were not able to distinguish any finer structure within the peak at 286 eV. We are not aware of any gas phase measurements of histidine but we can estimate the difference in 1s binding energy between the carboxylic acid carbon and the other carbon atoms in the following manner. Zhang et al.[36] have measured the spectra of a number of related aromatic amino acids, and the carboxylic acid C 1s binding energy is between 294.6 and 294.85 eV. Wickrama Arachchilage et al.[39] have measured the photoemission spectrum of a histidine containing dipeptide, and the C 1s binding energies of the atoms in the imidazole side chain vary from 291.0 to 292.0 eV. The weighted average difference (two states contribute to the 292 eV feature), is 3.1 eV. In our case the BE energy difference between the carboxylate component at 288.7 eV and the maximum of the broad peak (286 eV) is 2.7 eV, which is lower than the estimated value for histidine in the gas phase. This chemical shift is clearly due to chemisorption of histidine on the surfaces through the carboxylate group. As for the epitaxial CeO_2[27], the anionic bonding of histidine is observed for the polycrystalline cerium oxide film where oxygen atoms of the COO^- group bind to Ce cations on the surface. A significant difference from the previously published results on the epitaxial system is the ratio of areas of the two C 1s components measured with photon energy of 410 eV, corresponding to a highly surface sensitive condition (kinetic energy of photoelectrons about 120 eV). For histidine on the polycrystalline ceria after adsorption and 100° C annealing, it is equal to 8.5 instead of the value of 5 expected from stoichiometry. Moreover the ratio C 1s (COO^-) to C 1s (other

carbon atoms) calculated from data measured with 1486.6 eV photon energy is 1 to 5. As the integrity of the deposited molecules was checked on the reference Cu(111) substrate we conclude that the signal of the carboxylate group is attenuated by the rest of the molecule in the adlayer, that is, the carboxylate is close to the surface and the amino and IM groups are above it. This hypothesis was checked by estimating the attenuation of the COO^- signal by the molecule assuming a thickness of 4 Å. The value is 1.6, i.e. the ratio of areas is expected to be about 8, which is close to our measured value of 8.5.

The treatment at 100° C causes a shift of both components to lower binding energy by about 0.15 eV, i.e. the same value but different direction compared to the N 1s core level. Such a shift can be a result of intermolecular charge redistribution within the hydrogen bonded network. Annealing at 150° C and higher temperature substantially influences the C 1s peak, for instance decreasing the COO^- area, and confirms molecular decomposition. We do not see any sign of the component observed previously for histidine on CeO_2(111)/Cu(111) [27] in the valley at 287.8 eV which was attributed to the carbon adjacent to the α amino side group (C2 according to Fig. 1) bound to the O^{2-} (Ce^{3+}) centers. Thus the disordered histidine adlayer is bound to the oxide mainly through the carboxylate group.

The O 1s core level is difficult to analyze because of the intense signal from the oxide substrate with respect to carboxylate oxygen atoms of histidine and variations in the hydroxyl group concentration on the surface. The clean oxide has a main oxygen peak at 529.5 eV with a small shoulder at 531.1 eV (see Fig. 5c) owing to adsorbed OH groups on the grain edges and other imperfections of Ce^{3+} character. [40] Histidine adsorption causes the appearance of an additional component centered at 532 eV along with attenuation of the lattice oxygen signal. The O 1s core level was fitted using two Gaussian components centered at 529.5 and 532 eV. Their intensity variation together with total O 1s signal measured at photon energy 1486.6 eV are shown in Fig. 3c at different experimental steps. The decrease of the lattice oxygen signal at 529.5 eV after histidine adsorption is substantial especially for O 1s measured with 630 eV photons compared to data

acquired with 1486.6 eV photons (see Fig. 3c, red and blue marks on vertical axis). In the former case (excitation energy 630 eV), the photoelectrons have a kinetic energy of 100 eV and reflect the change in the oxygen concentration within the first ~0.5 -0.8 nm, i.e. real surface changes. Instead, the O 1s photoelectrons, measured with photon energy 1486.6 eV, of 956 eV kinetic energy have an information depth of ~1.5 nm. Interaction with histidine at 25° C causes the depletion of the oxygen in the top surface layers of the polycrystalline ceria film, i.e. surface reduction. The component at 529.5 eV slightly increases after annealing at 100° C of the histidine adlayer on CeO_2 while the total intensity of the O 1s measured with 1486.6 eV photons decreases. This indicates oxygen diffusion from the bulk of the oxide film towards the surface, or diffusion of vacancies into the bulk. Flashing to 100° C also reduces the width of the peak at 532.2 eV, mainly from the low BE side, where OH groups are contributing. This indicates oxygen loss from the surface which causes significant ceria reduction. Most likely the oxygen desorbs from the surface in the form of water and reduces the surface; this is characteristic of the polycrystalline ceria film [28] , and was not observed on the epitaxial layer. [27]

Combining all findings the following picture of histidine bonding to polycrystalline ceria can be drawn. Histidine binds to the surface through the two oxygen atoms of the carboxylate group and the release of the proton. The proton binds to the ceria surface oxygen forming an OH group and does not change the oxidation state of ceria cations. [41] The N K-edge NEXAFS spectra showed the absence of molecular ordering on the oxide surface with the IM ring unbound. We exclude imino nitrogen interaction with the surface because the difference between the π^* resonances is 1.7 eV. The α amino side group is involved in the intermolecular hydrogen bonding between the IM rings of neighboring molecules. The imino N atom of the IM ring is likely to be attracted to either the amino N atom of the ring or the α amino. We suggest that the water desorption is the reason for strong film reduction which also affects the deeper layers of the oxide. Comparing the absolute change of the RER ratio for histidine on epitaxial [27] and polycrystalline ceria surfaces, higher surface reduction was observed on the latter. For CeO_2(111)/Cu(111) it results in a RER ratio of

0.19 after histidine adsorption. It was attributed to the charge exchange between the IM ring p electrons and the f, d Ce orbitals. For the polycrystalline cerium oxide film the surface reduction was more pronounced (RER of 0.65 after histidine adsorption), the IM ring was not bound to the surface, and the C 1s component of the carboxylate group was at the same energy as for histidine/CeO_2(111)/Cu(111) – all these data confirm the suggestion that the water desorption from the surface is the result of polycrystalline ceria reaction with histidine. The high oxygen mobility of the polycrystalline oxide [28] facilitates oxygen diffusion for the reaction with the surface hydroxyl groups to form the water which desorbs.

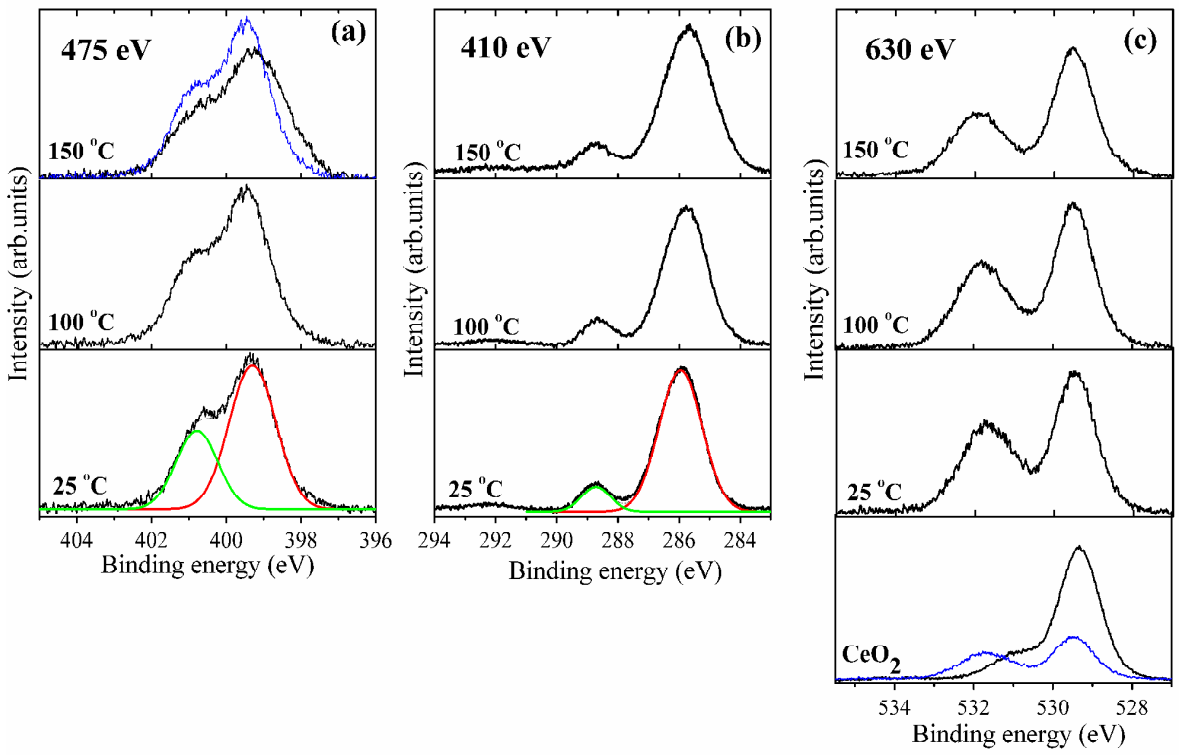

Fig. 5. (a) N 1s, (b) C 1s and (c) O 1s core levels of histidine adlayer on CeO_2 film, heated to 100° C and 150° C. The blue line in the upper panel of (a) is the spectrum after 100° C, shown for intensity comparison. An example of the N 1s and C 1s spectra fitting is shown for as deposited histidine adlayer in (a) and (b). The lowest panel in (c) shows the signal from the clean CeO_2 substrate before (black line) and after (blue line) histidine adsorption.

Conclusions

The bonding of histidine to the surface of polycrystalline cerium oxide thin films was studied by synchrotron radiation photoelectron spectroscopy, resonant photoelectron spectroscopy and near edge X-ray absorption fine structure spectroscopy. It was shown that histidine binds to CeO_2 in the anionic form His^- through the carboxylate group. The saturated molecular adlayer is disordered with the imidazole ring involved in intermolecular hydrogen bonding. The α-amino group binds via hydrogen atoms either to the oxide surface or to the IM ring of neighboring molecules. The polycrystalline structure of the oxide film is an important factor which determines the mechanism of histidine adsorption on the cerium oxide. Compared with well-characterized epitaxial films, the present system shows a number of similarities, for example in the core level photoemission spectra. However differences arise because of the polycrystalline nature of the thin films, particularly in the NEXAFS and O 1s spectra. There is a higher concentration of hydroxyl groups, the IM group is disordered and does not bond to the surface (in contrast to the epitaxial case), and the oxide surface is more reduced. On both surfaces bonding occurs via the carboxylate group. Cerium oxide functionalized by histidine can potentially contribute to the future development of biocompatible systems based on CeO_2 as an electrode material for metal ion sensors, or a model substrate for coordinated metal complexes.

Acknowledgement

The Materials Science Beamline is supported by the Ministry of Education of Czech Republic under Grant No. LG12003. We gratefully acknowledge the assistance of our colleagues at Elettra for providing good quality synchrotron light. We thank T. Skála for technical assistance.

References

1 P. A. Serra *Biosensors*; InTech: Croatia, 2010.

2 M. M. Rahman, A. J. S. Ahammad, J.-H. Jin, S. J. Ahn and J.-J. Lee, *Sensors*, 2010, **10**, 4855.

3 P. R. Solanki, A. Kaushik, V. V. Agrawal and B. D. Malholta, *NPG Asia Mater*, 2011, **3**, 17.

4 B. Chertok, M. J. Webber, M. D. Succi and R. Langer, *Mol. Pharmaceutics*, 2013, **10**, 3531.

5 M. Irimia-Vladu, *Chem. Soc. Rev.*, 2014, **43**, 588.

6 Sh. Saha, S. K. Arya, S. P. Singh, K. Sreenivas, B. D. Malhotra and V. Gupta, *Biosens.Bioelectron.*, 2009, **24**, 2040.

7 P. R. Solanki, C. Dhand, A. Kaushik, A. A. Ansari, K. N. Sood and B. D. Malhotra, *Sensor. Actuat. B-Chem.*, 2009, **141***,* 551.

8 A. A. Ansari, A. Kaushik, P. R. Solanki and B. D. Malhotra, *Electrochem. Commun.*, 2008, **10**, 1246.

9 A. A. Ansari, P. R. Solanki and B. D. Malhotra, *J. Biotechnol.*, 2009, **142**, 179.

10 A. K. Yagati, T.Lee, J. Min and J.-W. Choi, *Biosens. Bioelectron.*, 2013, **47**, 385.

11 R. E. Özel, C. Ispas, M. Ganesana, J. C. Leiter and S. Andreescu, *Biosens. Bioelectron.*, 2014, **52**, 397.

12 A. L. Bhatia, *Asian J. Exp. Sci.*, 2008*,* **22**, 33.

13 R. W. Tarnuzzer, J. Colon, S. Patil and S. Seal, *Nano Lett.*, 2005, **5**, 2573.

14 I. Celardo, J. Z. Pedersen, E. Traversa and L. Ghibelli, *Nanoscale*, 2011, **3**, 1411.

15 A. Y. Estevez, S. Pritchard, K. Harper, J. W. Aston, A. Lynch, J. J. Lucky, J. S. Ludington, P. Chatani, W. P. Mosenthal, J. C. Leiter, S. Andreescu and J. S. Erlichman, *Free Radical Bio. Med.*, 2011, **51**, 1155.

16 F. Pagliari, C. Mandoli, G. Forte, E. Magnani, S. Pagliari, G. Nardone, S. Licoccia, M. Minieri, P. Di Nardo and E. Traversa, *ACS Nano*, 2012, **6**, 3767.

17 K. Shikama, *Prog. Biophys. Mol. Bio.*, 2006, **91**, 83.

18 Y. Yuan, V. Simplaceanu, N. T. Ho and Ch. Ho, *Biochemistry*, 2010, **49**, 10606.

19 K. P. Kepp and P. Dasmeh, *J. Phys. Chem. B*, 2013, **117**, 3755.

20 C. Tanford, *J. Am. Chem. Soc.*, 1952, **74**, 211.

21 E. Chow and J. J. Gooding, *Electroanalysis,* 2006, **18**, 1437.

22 U. E. Wawrzyniak, P. Ciosek, M. Zaborowski, G. Liu and J. J. Gooding, *Electroanal.*, 2013, **25**, 1461.

23 L. Malachowski and J. A. Holcombe, *Anal. Chim. Acta*, 2003, **495**, 151.

24 W. Hieringer, K. Flechtner, A. Kretschmann, K. Seufert, W. Auwärter, J. V. Barth, A. Görling, H.-P. Steinrück and J. M. Gottfried, *J. Am. Chem. Soc.*, 2011, **133**, 6206.

25 A.-M. Andringa, M.-J. Spijkman, E. C. P. Smits, S. G. J. Mathijssen, P. A. van Hal, S. Setayesh, N. P. Willard, O. V. Borshchev, S. A. Ponomarenko, P. W. M. Blom and D. M. de Leeuw, *Organic Electronics*, 2010, **11**, 895.

26 K. Salazar-Salinas, L. A. Jauregui, C. Kubli-Garfias and J. M. Seminario, *J. Chem. Phys.*, 2009, **130**, 105101.

27 N. Tsud, R. G. Acres, M. Iakhnenko, D. Mazur, K. C. Prince and V. Matolín, *J. Phys. Chem. B*, 2013, **117**, 9182.

28 A. Migani, G. N. Vayssilov, S. T. Bromley, F. Illas and K. M. Neyman, *Chem. Commun.*, 2010, **46**, 5936.

29 M. Václavů, I. Matolínová, J. Mysliveček, R. Fiala and V. Matolín, *Journal of The Electrochemical Society*, 2009, **156**, B938.

30 V. Matolín, V. Johánek, M. Škoda, N. Tsud, K. C. Prince, T. Skála and I. Matolínová, *Langmiur*, 2010, **26**, 13333.

31 T. Skala, F. Šutara, K. C. Prince and V. Matolín, *J. Electron Spectrosc.*, 2009, **169**, 20.

32 http://www.kolibrik.net/science/kolxpd/

33 M. Nyberg, M. Odelius, A. Nilsson and L. G. M. Pettersson, *J. Chem. Phys.*, 2003, **119**, 12577.

34 V. Feyer, O. Plekan, N. Tsud, V. Lyamayev, V. Cháb, V. Matolín, K. C. Prince and V. Carravetta, *J. Phys. Chem. C*, 2010, **114**, 10922.

35 O. Plekan, V. Feyer, R. Richter, M. Coreno, M. de Simone, K. C. Prince and V. Carravetta, *Chem. Phys. Lett.*, 2007, **442**, 429.

36 W. Zhang, V. Carravetta, O. Plekan, V. Feyer, R. Richter, M. Coreno and K. C. Prince, *J. Chem. Phys.*, 2009, **131**, 35103.

37 Y. K. Gao, F. Traeger, O. Shekhah, H. Idriss and C. Wöll, *Journal of Colloid and Interface Science*, 2009, **338**, 16.

38 G. J. Fleming, K. Adib, J. A. Rodriguez, M. A. Barteau, J. M. White and H. Idriss, *Surf. Sci.*, 2008, **602**, 2029.

39 A. P. Wickrama Arachchilage, F. Wang, V. Feyer, O. Plekan and K. C. Prince, *J. Chem. Phys.*, 2012, **136**, 124301.

40 Y. Lykhach, V. Johánek, H. A. Aleksandrov, S. M. Kozlov, M. Happel, T. Skála, P. St. Petkov, N. Tsud, G. N. Vayssilov, K. C. Prince, K. M. Neyman, V. Matolín and J. Libuda, *J. Phys. Chem. C*, 2012, **116**, 12103.

41 Y. Lykhach, T. Staudt, M. Vorokhta, T. Skála, V. Johánek, K. C. Prince, V. Matolín and J. Libuda, *J. Catal.*, 2012, **285**, 6.

TOC Graphic